Supplement material for the manuscript:

Mid-Holocene rainfall changes in the southwestern Pacific

By Cinthya Nava-Fernandez et al.

Supplement 1. Correlation of oxygen and carbon isotopes in stalagmite C132.

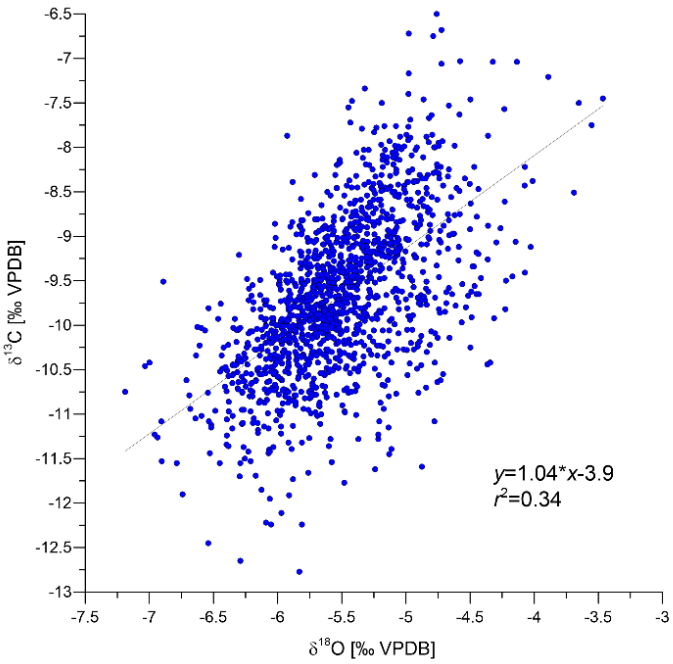

Fig. S1. Stalagmite C132 oxygen and carbon isotope ratios correlate in both, high and low resolution data sets.

Supplement 2. PCAs of the trace elements records at high resolution (30 µm).

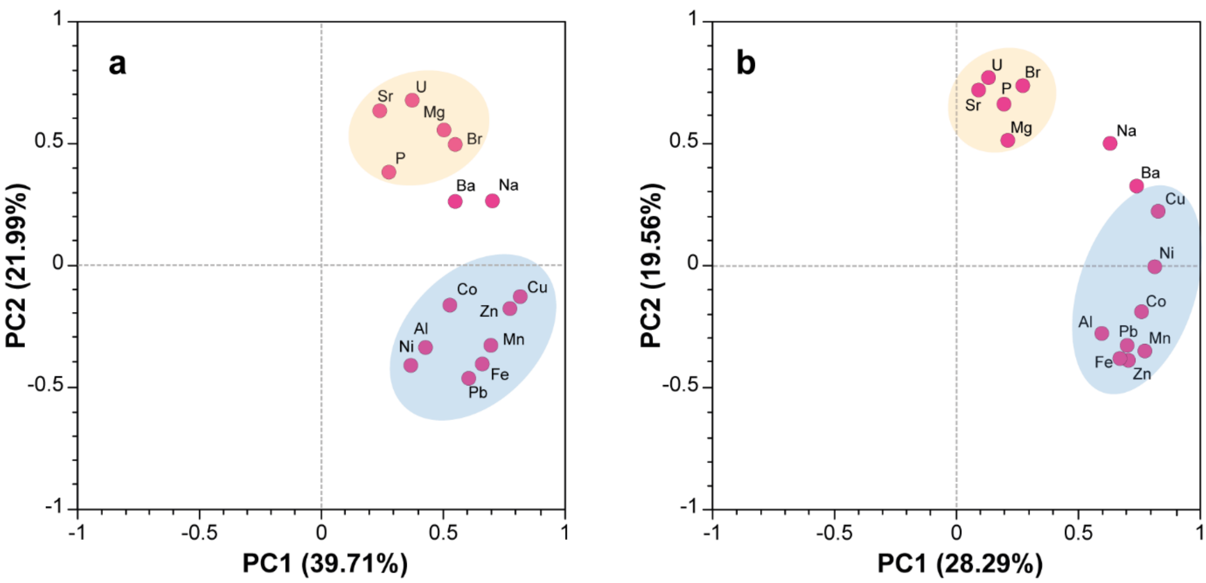

Fig. S2. Results of principal component analyses. a) PCA-3a, and b) PCA-3b. Two clusters are evident: group 1 is formed by Zn, Mn, Fe, Pb, and Al (blue shaded area), and group 2 comprises Sr, Mg, U and P (orange shaded area).

Supplement 3. Seasonality reconstruction

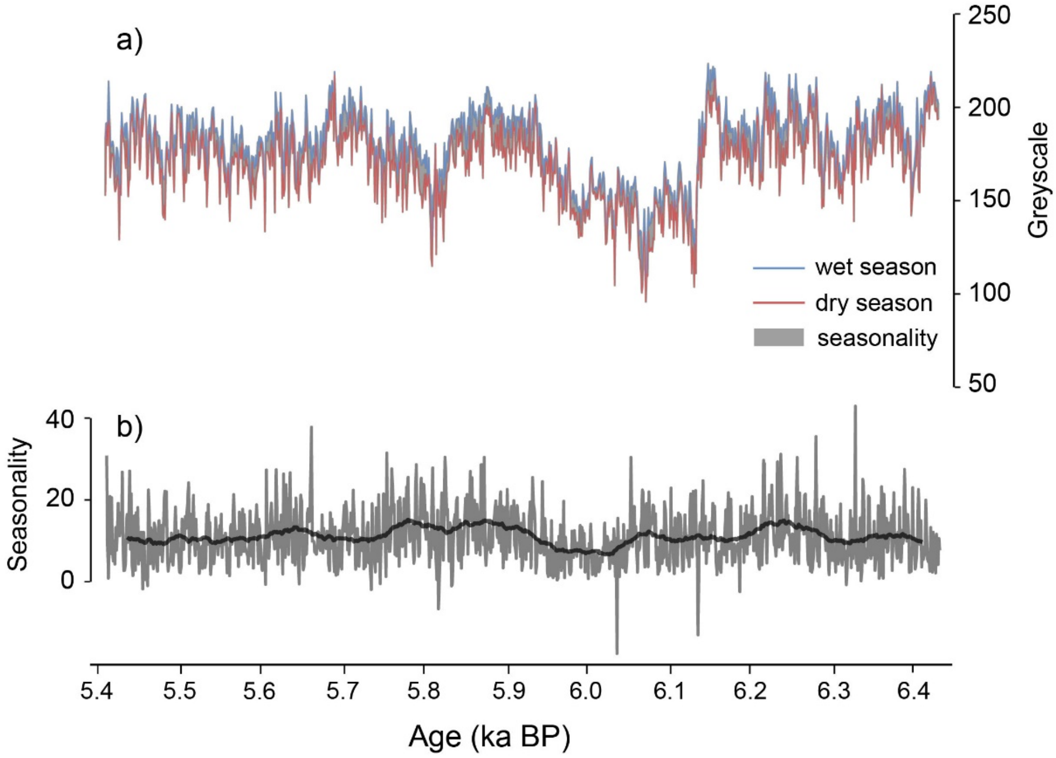

Fig. S3. a) seasonality (grey area) derived from the difference between the wet (blue line) and dry season (red line). b) seasonality record (grey line) and its running average (black line).

Supplement 5. Recurrence plots

Recurrence plots (RPs) are a powerful nonlinear time series analysis tool. In several applications, RPs have been effectively applied for the detection of abrupt transitions in palaeoclimate records (Westerhold et al., 2020). An RP is represented by a symmetric 2-dimensional binary matrix (see S5) in which each black dot denotes a recurrence between the states of the system at two times i and j while white dots mark no recurrences. The notion of recurrence is based on a distance measure (e.g., Euclidean distance) between the amplitudes of the studied time series at times i and j. In the study of nonlinear dynamical systems, a univariate time series often has to be regarded as a series of 1-dimensional observations of an underlying (but unknown) higher dimensional system, represented by a phase space trajectory. In order to obtain an RP that is based on this phase space representation of the system, time-delay embedding is the most common method to reconstruct the unknown phase space. To obtain RPs for the different segments of the seasonality time series, we estimated the embedding delay as the first zero-crossing of the autocorrelation $(\tau = 2)$ and the embedding dimension by the false nearest neighbour-algorithm $(m = 3)$ (Kantz and Schreiber, 2004). Using these embedding parameters, the time series was split into 200 yrs.-windows and an RP was computed for each embedded time series segment with a fixed recurrence rate of 15%. RPs exhibit different line structures that can be interpreted in context of the variability of the time series and which are often used to obtain quantitative measures of recurrence characteristics (Marwan et al. 2008). Diagonal lines reflect predictable dynamics whereas their length can be interpreted as a proxy for the predictability time of the system. To obtain an indicator of seasonal predictability, we analysed the occurrence of diagonal lines in each RP by the determinism measure DET which is defined as the fraction of diagonal lines exceeding a specified minimum length

$(l = 2)$. Significance was assessed by bootstrap resampling of diagonal lines as described in Marwan et al. (2008). Two exemplary RPs are shown in fig. S5.

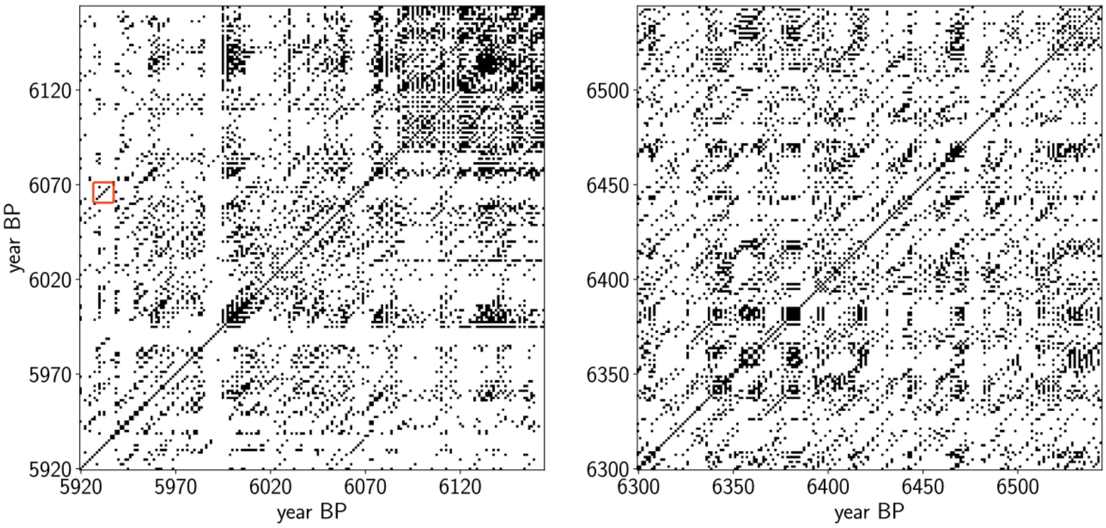

Fig. S5. Two exemplary recurrence plots that yield distinct determinism parameter DET values for the respective time periods, i.e., DET=0.28 (left) and DET = 0.23 (right). Both axes are time axes. Black dots mark recurrences between similar states. DET quantifies the number of diagonal lines that exceed a certain minimum line length (l_{min} = 2 years). An exemplary diagonal line of length l_{min} = 6 years is highlighted by a red box and reflects six years of predictable seasonal variations.

Supplement 4. Wavelet spectral analysis of the PCA-2.

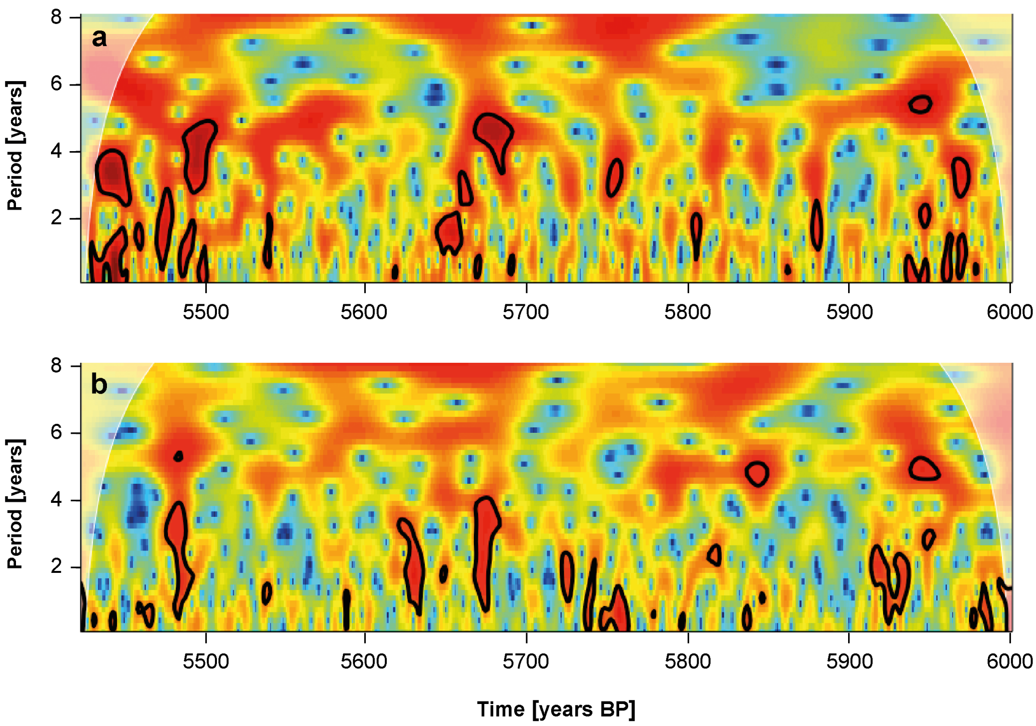

Fig. S4. Wavelet analysis of the principal components extracted from PCA-2 of the annually resolved C132 proxy records for the period of 6002 to 5422 years BP (a) PC1 and b) PC2). Significant periods are outlined in black.

Supplement 6. Correlation of rain and drip water oxygen and hydrogen isotope ratios.

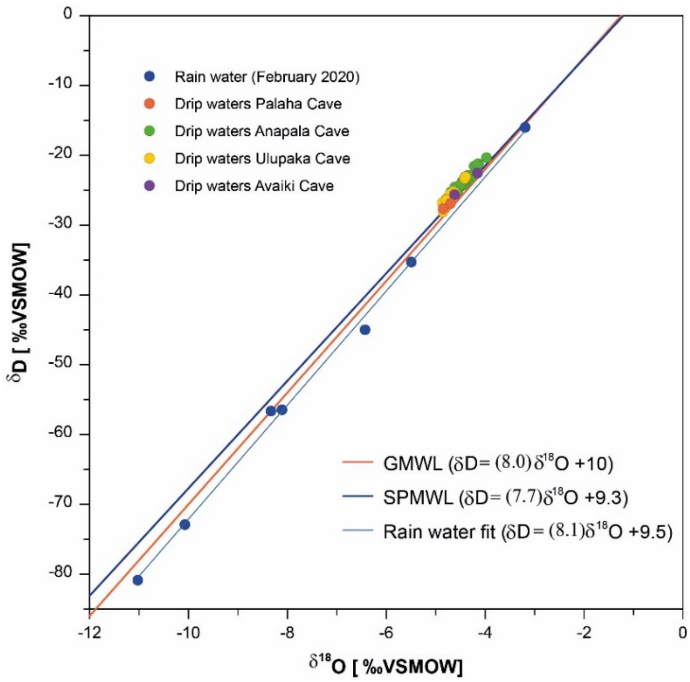

Fig. S6. Relationship between $\delta^{18}O$ and δD of Niue rain and dripwater collected in February 2020. Dripwaters were collected from Anapala Cave (inland), Palaha Cave (sea cave), Ulupaka Cave (inland) and Avaiki Cave (sea cave). The collected samples plot along the SPMWL ($\delta D = 7.7 * \delta^{18}O + 9.3$) derived from rainfall data of neighboring Western Samoa and Rarotonga stations (IAEA/WMO, 2001) and show no signs of secondary evaporation.

Technical details of the Methods

Speleothem stable isotope analyses at ETH Zurich

Between 90 and 140 µg of sample powder was reacted with orthophosphoric at 70°C for 60 min. The resulting CO_2 was then sampled and transported in a helium stream to the mass spectrometer. Details on the methods can be found in Breitenbach and Bernasconi, 2011). Reference materials include the international standards NBS19 and NBS18. The long-term 1σ reproducibility of the internal standard is 0.05 ‰ for $\delta^{13}C$ and 0.08 ‰ for $\delta^{18}O$.

LA-ICP-MS device specifications

Analyses were conducted using a laser repetition rate of 20 Hz with a 60 µm diameter ablation spot and scanning the sample at 29.55 µm/sec with a beam energy density of 5 J/cm^2, yielding a spatial resolution of 30 µm. Signals for ^{23}Na, ^{24}Mg, ^{27}Al, ^{29}Si, ^{31}P, ^{34}S, ^{44}Ca, ^{55}Mn, ^{56}Fe, ^{60}Ni, ^{63}Cu, ^{66}Zn, ^{88}Sr, ^{137}Ba, ^{208}Pb, and ^{238}U were monitored during analysis in a single track. The ICP-MS was optimised daily for maximum sensitivity. The ICP-MS operating settings are: forward power of 1350 watts, plasma gas flow rate of 15 L/min (Ar), carrier gas flow of 0.99 mL/min (nebuliser), sampling depth of 4 mm, pulse counting detector and peak hopping sweep mode, 0.01-0.1 s dwell time and one point per peak 1. Calcium was used as internal standard, assuming a concentration of 40.04 wt%. Background counts (He gas background, measured with the laser off) were collected for 45 seconds between samples. NIST (National Institute of Standards and Technology) glass standards 612 and 610 were analysed after every sample track (ca. 3 cm long) to account for any drift. Raw data were processed using Iolite v3.32 (Paton et al., 2011). Background counts were subtracted from the raw data and all data were standardised to

NIST 612. NIST 610 was utilised as a secondary standard. The GeoReM database (Jochum et al., 2005) was used for NIST glass reference values.

Spectral analysis

The continuous wavelet analysis of the greyscale record (Fig. 6a), utilised linear interpolation with a sampling time of one year. Irregular sampling in the time dimension results in variations in the number of samples per year, biasing estimates of mean season-specific rainfall, a problem that is not resolved by interpolation. Significance testing of wavelet power was thus based on Monte-Carlo sampling of AR(1)-realisations computed by the REDFIT algorithm (Schulz and Mudelsee, 2002) to obtain an individual 95% confidence level for each time instance and period. The same procedure was applied to the seasonality time series (Fig. 6b) by transforming each AR(1)-surrogate into a 'seasonality-surrogate'.

Recurrence analysis

Diagonal lines in a RP reflect deterministic variations in a time series which can be characterised by the determinism parameter DET (S5). We characterised the seasonal-scale predictability by computing a DET value for each RP (Fig. 7g), and tested the hypothesis that no significant shift in DET has occurred over the covered period following the bootstrapping approach proposed by (Marwan et al., 2008).

References

Breitenbach, S. F. M. and Bernasconi, S. M.: Carbon and oxygen isotope analysis of small carbonate samples (20 to 100 µg) with a GasBench II preparation device, Rapid Commun. Mass Spectrom., 25(13), 1910–1914, doi:10.1002/rcm.5052, 2011.

Jochum, K. P., Nohl, U., Herwig, K., Lammel, E., Stoll, B. and Hofmann, A. W.: GeoReM: A new geochemical database for reference materials and isotopic standards, Geostand. Geoanalytical Res., 29(3), 333–338, doi:10.1111/j.1751-908x.2005.tb00904.x, 2005.

Kantz, H. and Schreiber, T.: Nonlinear Time Series Analysis, Second ed., edited by C. University Press., 2004.

Marwan, N., Schinkel, S. and Kurts, J.: Significance for a recurrence based transition analysis, Int. Symp. Nonlinear Theory its Appl. NOLTA'08, Budapest, Hungary, (3), 412–415, 2008.

Paton, C., Hellstrom, J., Paul, B., Woodhead, J. and Hergt, J.: Iolite: Freeware for the visualisation and processing of mass spectrometric data, J. Anal. At. Spectrom., 26(12), 2508–2518, doi:10.1039/c1ja10172b, 2011.

Schulz, M. and Mudelsee, M.: REDFIT: Estimating red-noise spectra directly from unevenly spaced paleoclimatic time series, Comput. Geosci., 28(3), 421–426, doi:10.1016/S0098-3004(01)00044-9, 2002.

Westerhold, T., Marwan, N., Drury, A. J., Liebrand, D., Agnini, C., Anagnostou, E., Barnet, J. S. K., Bohaty, S. M., De Vleeschouwer, D., Florindo, F., Frederichs, T., Hodell, D. A., Holbourn, A. E., Kroon, D., Lauretano, V., Littler, K., Lourens, L. J., Lyle, M., Pälike, H., Röhl, U., Tian, J., Wilkens, R. H., Wilson, P. A. and Zachos, J. C.: An astronomically dated record of Earth's climate and its predictability over the last 66 million years, Science (80-.)., 369(6509), 1383–1388, doi:10.1126/SCIENCE.ABA6853, 2020.